



HAL
open science

Evaluation of four tumour growth models to describe the natural history of meningiomas

Julien Engelhardt, Virginie Montalibet, Olivier Saut, Hugues Loiseau,
Annabelle Collin

► **To cite this version:**

Julien Engelhardt, Virginie Montalibet, Olivier Saut, Hugues Loiseau, Annabelle Collin. Evaluation of four tumour growth models to describe the natural history of meningiomas. *EBioMedicine*, 2023, 94, pp.104697. 10.1016/j.ebiom.2023.104697 . hal-04346355

HAL Id: hal-04346355

<https://hal.science/hal-04346355>

Submitted on 15 Dec 2023

HAL is a multi-disciplinary open access archive for the deposit and dissemination of scientific research documents, whether they are published or not. The documents may come from teaching and research institutions in France or abroad, or from public or private research centers.

L'archive ouverte pluridisciplinaire **HAL**, est destinée au dépôt et à la diffusion de documents scientifiques de niveau recherche, publiés ou non, émanant des établissements d'enseignement et de recherche français ou étrangers, des laboratoires publics ou privés.

EVALUATION OF FOUR TUMOUR GROWTH MODELS TO DESCRIBE THE NATURAL HISTORY OF MENINGIOMAS

Julien Engelhardt^{1,2}, Virginie Montalibet², Olivier Saut², Hugues Loiseau¹, Annabelle Collin²

1. Service de Neurochirurgie B, CHU de Bordeaux, Place Amélie Raba-Léon, 33076
Bordeaux Cédex, France

2. Univ. Bordeaux, Inria Bordeaux-Sud-Ouest, Bordeaux INP, CNRS, IMB, UMR 5251, F-33400, Talence, France

ABSTRACT

Background

The incidence of newly diagnosed meningiomas, particularly those diagnosed incidentally, is continually increasing. The indication for treatment is empirical because, despite numerous studies, the natural history of these tumors remains difficult to describe and predict.

Methods

This retrospective single-centre study included 294 consecutive patients with 333 meningiomas who underwent three or more brain imaging scans. Linear, exponential, power, and Gompertz models were constructed to derive volume-time curves, by using a mixed-effect approach. The most accurate model was used to analyse tumour growth and predictors of rapid growth.

Findings

The Gompertz model provided the best results. Hierarchical clustering at the time of diagnosis and at the end of follow-up revealed at least three distinct groups, which can be described as pseudoexponential, linear, and slowing growth with respect to their parameters. Younger patients and smaller tumors were more frequent in the pseudo-exponential clusters. We found that the more “aggressive” the cluster, the higher the proportion of patients with grade II meningiomas and who have had a cranial radiotherapy. Over a mean observation period of 56.5 months, 21% of the tumours moved to a cluster with a lower growth rate, consistent with the Gompertz’s law.

Interpretation

Meningiomas exhibit multiple growth phases, as described by the Gompertz model. The management of meningiomas should be discussed according to the growth phase, comorbidities, tumour location, size, and growth rate. Further research is needed to evaluate the associations between radiomics features and the growth phases of meningiomas.

Funding

No funding sources.

Keywords:

Meningioma, Gompertz model, natural history, volumetry

RESEARCH IN CONTEXT

Evidence before this study

The first case series of incidental meningiomas was published in 1990. Since then, several studies have evaluated the natural history of meningiomas. A first type of studies analysed radiological progression-free survival to identify predictors of tumour growth, albeit with conflicting results. Fluid-attenuated inversion recovery (FLAIR) hyperintensity, peritumoral oedema, and tumour size are possible risks factors for tumour growth, whereas older age and calcifications are negatively correlated with tumour progression. However, previous studies differed in terms of the indicators of progression, measurement methods (planar or volumetry), and accuracy. A literature review of 20 studies (2,130 patients) with a median follow-up duration of 49.5 months showed differences among the studies in terms of the monitoring of meningioma growth; therefore, a meta-analysis could not be performed. A second type of studies evaluated growth rates between the first and final imaging scans to identify predictors of rapid growth. Despite conflicting results, the studies found that older age, male sex, an isointense or hyperintense FLAIR signal, peritumoral oedema, and tumour size were associated with a high tumour growth rate (TGR), whereas calcifications and a skull base location were negatively associated with the growth rate. Based on these factors, two retrospective studies developed the Asan Intracranial Meningioma Scoring System and IMPACT risk scores. However, to our knowledge, no previous prospective study has validated the risk scores in an independent cohort. Furthermore, previous studies differed in terms of the growth rate

calculation method (linear or exponential approximations) and definition of rapid progression. A third type of studies have shown that meningiomas exhibit varying growth patterns over time. One study showed that grade I meningiomas may exhibit linear or exponential growth, or no growth at all, whereas grade II meningiomas exhibit exponential growth. A later study showed that the various growth patterns might reflect a general law of tumour kinetics, where meningioma growth may follow a logistic or Gompertzian growth pattern. A non-linear approach has been used to estimate model parameters; this requires a sufficient follow-up duration and low-noise observations, which leads to selection bias in favour of slow-growing and small tumours that may impact the reproducibility of the results. To overcome this issue, in a preliminary study, we estimated model parameters using a mixed-effect (population) approach and found that the Gompertz model was more accurate than the linear model for predicting the volumetric evolution in incidental meningiomas.

Added value of this study

To our knowledge, the present study is the largest case series ($n = 333$) of consecutive patients with incidental meningiomas. Moreover, the patients were followed-up for a mean duration of 56.5 months and underwent a median of three imaging scans after diagnosis. The population approach was superior to the non-linear regression model (individual approach) in terms of robustness and accuracy. Using the population approach to estimate the model parameters, we showed that the Gompertz model was more accurate for predicting the natural history of meningiomas than linear, exponential, and power models. The sample size and parameter estimation methods are important for modelling, statistical comparison of models, representativeness, and reproducibility. Then, hierarchical clustering was performed at diagnosis and the end of follow-up to determine the tumour growth patterns (pseudo-exponential, linear, and slow growth) described previously, that correspond to different phases of the Gompertz curve. During the follow-up period, 21% of the tumours moved to a cluster with a lower growth rate, which is consistent with the Gompertz law. Finally, we showed that patient age and tumour volume at diagnosis were significantly associated with the growth pattern. Younger age and small tumour size were associated with the pseudo-exponential cluster. More “aggressive” clusters were associated with a greater likelihood of cranial radiotherapy prior diagnosis and World Health Organization (WHO) grade II meningiomas. However, there were no significant associations among the FLAIR signal, peritumoral oedema, calcifications, and growth patterns.

Implications of the available evidence

The growth rate of meningiomas is not constant and is well described by the Gompertz model. Therefore, dichotomous classification of meningiomas as more or less aggressive based on the average TGR computed from the first and last imaging scans, or radiological progression alone, may be inaccurate. The management of meningiomas should be based on the growth pattern, tumour location, size, and growth rate, and comorbidities. Further research using radiomics techniques is needed to predict the growth phase based on the initial imaging features.

INTRODUCTION

Meningiomas account for the most frequent intracranial tumors¹. Their annual incidence rate is around 7 and 9/100 000¹ with a significant increase between 1 and 6%/year according to some brain tumor registries² leading to an increasing part of healthcare consumption (monitoring brain imaging and specialized consultations repeated over a long period of time). The rationale of treating incidental meningiomas is to prevent neurological symptoms³ (focal deficit or cognitive impairment due to compression of neural structures, epilepsy, intracranial hypertension) and thus depends on their expected evolution over time.

Numerous studies have explored the natural history of meningiomas (for review, see⁴), with varying tumor size measurement methods. The data that emerged are that meningiomas show variable growth profiles and that some clinical and radiological features could be linked to tumor progression or rapid growth, provided that these terms can be defined univocally. However, these tumors are followed up through a rather small window of time in comparison with their entire "life"⁵; and the different growth patterns described on different individuals may be the parts of a more general tumor kinetics law.

In parallel, tumor growth kinetics has been an object of mathematical study for more than a half century⁶. The exponential model is the simplest; however, it cannot explain the variability in the tumour growth rate (TGR) over time and is theoretically unacceptable because it posits unlimited tumour growth⁷. Therefore, the Gompertz model has been used to explain the growth rate of certain tumours,⁷⁻¹⁰ the power model has also been used, particularly for malignant tumors¹¹. However, the main difficulty with these models is the estimation of the parameters to fit the data. Ideally, fitting is done for each individual tumour, but this requires a long follow-

up duration and low-noise observations, which is only possible in experimental settings and cases of slow-growing or small tumours; this might lead to selection bias in studies of the natural history of meningiomas.¹² To overcome this issue, model parameters may be estimated using the population approach (or mixed-effect models¹³), provided that the population is large and representative.

In a previous study¹⁴ of 39 meningiomas, we tested this original approach, and we showed that the Gompertz model was more accurate than linear modelling in describing and predicting the evolution of incidental meningiomas. In the present study, the primary objective was to verify these encouraging results and to compare the ability of the four most commonly used models (linear, exponential, power, and Gompertz) to analyse tumour growth in a larger cohort using a population approach. The secondary objective was to explore clinical and radiological predictors of growth patterns based on the most accurate model

PATIENTS AND METHODS

Presentation of the study and clinical data

Study design and participants

In this retrospective study, we analysed data from consecutive adult patients with incidental meningioma who were referred to one of the investigators (H.L.) for a neurosurgery consultation between December 2013 and August 2021. The patients attended regular clinical and radiological follow-up visits. The patients were treated based on volumetric progression or neurological symptoms as done in daily practice after approval by the tumour board.

Procedure and variable extraction

We recorded the age at diagnosis, sex, number of meningiomas (classified as solitary or multiple), tumour location, prior cranial radiotherapy, prior and current hormonal treatment, T2 or FLAIR signal changes (hypointensity, isointensity, or hyperintensity compared to the grey matter signal), calcifications (presence or absence), peritumoral oedema (presence or absence), treatment date, and modality. We used these data to calculate the Asan Intracranial Meningioma Scoring System (AIMSS) risk score for each tumor.¹⁵ All the imaging (MRI scans with 3D millimetric T1 WI sequence with gadolinium or CT-scans with contrast product injection if

contra-indications to MRI) were segmented by the same senior neurosurgeon (HL) using Sophia Radiomics© software. This software contains a semi-automatic 3D segmentation algorithm that allows obtaining a tumor mask that is then corrected and validated by the investigator. To verify the accuracy of the volumetric measurements, we selected 11 meningiomas and performed the measurements again, by the same investigator (HL) and another one (JE). The detailed methodology and results are described in the supplementary material, part I.

Inclusion and exclusion criteria for mathematical modeling

Only tumours for which at least three scans were acquired at different time points were included. We excluded patients with missing baseline data, as well as those treated with cyproterone, noregestrol, or chlormadinone acetate at the time of the meningioma diagnosis, those with type 2 neurofibromatosis, and those showing a statistically significant decrease in tumour volume over time as defined in the paragraph “Statistical analysis”.

Modeling of meningiomas evolution

Mean growth rate during the observation period

To compare our results with previously published data, we estimated the mean growth rate during the follow-up period, i.e. from the time of diagnosis (t_0) to the last available time point (t_{last}), for which the corresponding tumour volumes were V_0 and V_{last} . The formula for linear approximation of the annual growth rate (AGR; cm³/year) is as follows:

$$AGR = \frac{V_{last} - V_0}{t_{last} - t_0}$$

The formula for exponential approximation of the TGR (%/year) is as follows:

$$TGR = 100. \left[\left(\frac{V_{last}}{V_0} \right)^{\frac{1}{t_{last} - t_0}} - 1 \right]$$

The tumour doubling time (TDT; years) was calculated as follows:

$$TDT = \frac{\ln 2}{\ln \left(\frac{TGR}{100} + 1 \right)}$$

Mathematical models, fit procedure, and goodness of fit criteria

The aforementioned approximations of growth rate are based on linear or exponential modelling, and thus may be considered excessively simplistic; they model meningioma volumes only near t_0 and t_{last} . To overcome this limitation, mathematical modelling was

performed herein over the entire study period using four classical models of tumour growth. Variation in meningioma volume (cm³) as a function of time since diagnosis (months) was fitted using linear, exponential, power, and Gompertz models. We denote the estimated volume at time t as \hat{V} , estimated volume at first imaging t_0 as \hat{V}_0 , and model parameters as α , β , and γ :

1. Linear model

$$\hat{V}(t) = \hat{V}_0 + \alpha t, \quad \alpha > 0.$$

Where α is the slope of the growth. The more α is large, the more the tumour is growing rapidly.

2. Exponential model

$$\hat{V}(t) = \hat{V}_0 e^{\alpha t}, \quad \alpha > 0,$$

corresponding to the explicit solution of the ordinary differential equation: $\hat{V}' = \alpha \hat{V}$ with $\hat{V}(t_0 = 0) = \hat{V}_0$, where α is the growth rate (assumed to be constant). The more α is large, the more the tumour is growing rapidly.

3. Power model

$$\hat{V}(t) = ((\hat{V}_0)^{1-\gamma} + \alpha(1-\gamma)t)^{\frac{1}{1-\gamma}}, \quad 0 < \gamma < 1, \quad \alpha > 0,$$

corresponding to the explicit solution of the ordinary differential equation: $\hat{V}' = \alpha \hat{V}^\gamma$ with $\hat{V}(t_0 = 0) = \hat{V}_0$. This model is based on the hypothesis that the volume growth is proportional to a power - denoted by γ - of the volume. The proportionality coefficient is denoted by α . This model is a simplification of the classical Von Bertalanffy model, see the discussion section.

4. Gompertz model

$$\hat{V}(t) = \hat{V}_0 e^{\frac{\alpha}{\beta}(1-e^{-\beta t})}, \quad \alpha, \beta > 0$$

corresponding to the explicit solution of the ordinary differential equation: $\hat{V}' = \alpha e^{-\beta t} \hat{V}$ with $\hat{V}(t_0 = 0) = \hat{V}_0$. In this model, α is the initial growth rate and $\frac{1}{\beta}$ corresponds to the characteristic time at which the tumor growth capacity decreases. One can observe that if β equals to 0, we retrieve the exponential model. At a fixed initial growth rate α , the more β is large, the more the growth rate decreases quickly.

To estimate \hat{V}_0 , α , β , and γ , a population approach was used. The mixed-effects approach involves pooling the data of all patients together and estimating global distributions of the

model parameters. More precisely, the individual parameters α^j , β^j and γ^j , (where j denotes the individual) are assumed to be realizations of a random variable decomposed into two parts:

$$\log (\{\alpha, \beta\}^j) = \log (\{\alpha, \beta\}^{pop}) + \{\tilde{\alpha}, \tilde{\beta}\}^j, \text{logit}(\{\gamma\}^j) = \text{logit}(\{\gamma\}^{pop}) + \{\tilde{\gamma}\}^j,$$

where $\{\alpha, \beta, \gamma\}^{pop}$ corresponds to the fixed effects and $\{\tilde{\alpha}, \tilde{\beta}, \tilde{\gamma}\}^j$ corresponds to the random effects and have been assumed with mean zero. Models also depend on the initial volume \hat{V}_0^j . This value can be fixed with the volume computed using the first MRI examination denoted V_0^j but doing that does not allow to consider the uncertainty of the segmentation process. That is why we considered \hat{V}_0^j of each meningioma as a covariate of V_0^j :

$$\hat{V}_0^j = V_0^j(1 + e_0),$$

where e_0 follows a Gaussian law of mean zero and of standard deviation which is estimated. We assumed that the measurement error for all volumes is proportional. The standard deviation is estimated and is used to define the 95% confidence interval given in the fits.

In Supplementary Materials (Section III), an analysis with synthetic data was performed to justify our estimation approach. A comparison between the two approaches (population and individual), an evaluation of the robustness of the method even with not adapted parameter distributions, and an identification of the estimated quantities that appear reliable were performed. Of course, this does not mean that equivalent results can be obtained with real data: these are only some indications. Using an individual estimation for the real data leads to equivalent results for most meningiomas, but to very unrealistic behaviors for some of them, in particular a very large increase in growth rate six months later. In addition, the parameter distributions in the individual approach are close to the log-normal distribution. These different tests convince us that the mixed-effects approach is the better method in this context.

The goodness of fit of the models were compared by the Akaike (AIC) and the Bayesian information criterion (BIC). Given a set of candidate models for the data, the model with the lowest AIC value was the preferred model. The AIC rewards goodness of fit (as assessed by the likelihood function), but also includes a penalty that is an increasing function of the number of estimated parameters: $AIC = 2k - 2\ln(L)$, where k is the number of parameters and L is the maximum maximized value of the likelihood function. The penalty prevents overfitting, which is desirable because increasing the number of parameters in the model almost always improves the goodness of fit. The formula for BIC is similar to the formula for AIC, but with a different penalty for the number of parameters: $BIC = k \ln(n) - 2\ln(L)$ where n is the number of data

points. Comparing both criteria is beyond the scope of this paper, but many studies in the literature compare them, see for example ^{16,17}. In¹⁸, the author explains that AIC is better suited to model selection for prediction and that BIC is better suited to model selection for explanation. In this work, we chose a model with small AIC and BIC to take advantage of both criteria. For each individual meningioma j , we calculated the MSE (mean squared error) between the estimated and real volumes, since it is the value that is minimized and also the relative L^1 , L^∞ errors since they are informative data (L^∞ indicates the worst error, and L^1 gives an idea of the percentage error, see formulas of Section II in Supplementary material).

Analysis of the growth rate over time

The estimated volume \hat{V} was calculated for all time points using the indicated formulas. Then, we estimated the relative growth-rate (RGR; %) during X months before and after any time t as follows:

$$\text{RGR}_{-X}^j(t) = \frac{\hat{v}^j(t) - \hat{v}^j(t-X)}{\hat{v}^j(t)} \text{ and } \text{RGR}_{+X}^j(t) = \frac{\hat{v}^j(t+X) - \hat{v}^j(t)}{\hat{v}^j(t)} \text{ respectively.}$$

To estimate, if at this given time t , the RGR was increasing or decreasing, the following growth rate ratio (GRR) was calculated as follows:

$$\text{GRR}_X^j(t) = \frac{\text{RGR}_{+X}^j(t)}{\text{RGR}_{-X}^j(t)}.$$

Then, hierarchical clustering of the meningiomas was performed using RGR_{+X} and GRR_X . A dendrogram was constructed using the Ward.D2 agglomeration method (performed with the `hclust` function). In turn, the dendrogram was used to identify the optimal number of clusters.

Statistical analysis

Quantitative variables are presented as means \pm standard deviations or median (25th–75th percentile) and were compared using Student's t-test or the Mann–Whitney U test as appropriate. Multiple comparisons between groups were performed using analysis of variance (ANOVA or the Kruskal-Wallis' test, as appropriate). Qualitative variables are presented as absolute values with percentages and were compared using Fisher's exact test or the χ^2 test as appropriate, i.e., based on the number of observations. The associations of ordinal variables with other variables were analysed using Spearman's correlation coefficient. A statistically significant decrease in tumour volume over time was defined as a negative (within the 95%

confidence interval) linear regression coefficient. The model parameters were estimated using MonolixSuite 2020R1⁴⁰. Two-sided p-values < 0.05 were considered indicative of statistical significance. Analyses were performed using R software (R Foundation for Statistical Computing, Vienna, Austria).

Ethical considerations

This study was performed in compliance with the Declaration of Helsinki. All patients were informed about the study's purpose and informed consent was obtained from the participants and/or their legal guardians. The study protocol was approved by the Institutional Review Board.

Role of the funding source

No funding sources.

RESULTS

Patients and meningiomas

During the study period, 294 consecutive patients with 333 tumours fulfilled the study inclusion criteria (Supplementary Materials, Section IV, Figure S8). The clinical, radiological, and follow-up data are summarized in Table 1 and in Supplementary Materials, Section IV (Figure S9, tables S2 and S3).

Modeling of the volume variation over time

Figure 1 depicts six representative growth curves of meningiomas fitted with the four models. It illustrates how the Gompertz model seems the more accurate to fit the data in all cases. When calculating the goodness of fit criteria, the Power and Gompertz models gave similar results with close AIC and BIC and no significant difference between errors (Figure 2, Supplementary Materials Section IV, table S4). It can be seen that AIC and BIC are very different for the linear model. It is known that BIC penalizes the model complexity more. The difference is more important when AIC chooses a larger model than BIC. This means that the linear model is good for describing the data, but not for making predictions. Since we want to do both, we select models – Power and Gompertz models – with small AIC and BIC. The Power and Gompertz models gave significantly smaller errors than the linear one, but not than the exponential model.

Because the Gompertz model gave the best results in all the metrics used, it was selected to model the meningiomas growth in what follows. The standard deviation of the proportional error was estimated at 14.6%.

Tumor growth analysis according to the Gompertz model

The estimation of the parameters of the Gompertz model gave: $\log(a) \sim \mathcal{N}(-4.269, 0.006)$, $\log(b) \sim \mathcal{N}(-4.51, 0.89)$ and $e_0 \sim \mathcal{N}(0, 0.05)$. Analysis of the synthetic data showed that prediction at almost 6 months had the best balance between the prediction error, which increases over time, and the need to predict the volume over a sufficiently long period to detect a change in growth rate (see Section III of the Supplementary Materials). Furthermore, we estimated the RGR and GRR based on the first and last MRI scans (obtained at t_0 and t_{last} , respectively) with good accuracy. Based on these data, hierarchical clustering identified four clusters at t_0 (figure 3). Then, based on the GRR_6 and RGR_{+6} , we distinguished slow growth (cluster 1: $GRR_6 = 0.3$ [0.2–0.4]), linear (cluster 2: $GRR_6 = 1.0$ [0.9–1.0]), accelerating (cluster 3: $GRR_6 = 1.1$ [1.1–1.2] and $RGR_{+6} = 19.4\%$ [14.3–28.8]), and fast-accelerating (cluster 4: $GRR_6 = 1.6$ [1.4–1.9] and $RGR_{+6} = 79.1\%$ [53.7–102.8]) patterns. The hierarchical clustering also identified three patterns at t_{last} (Figure 3), namely slow growth (cluster 1: $GRR_6 = 0.3$ [0.2–0.5]), linear (cluster 2: $GRR_6 = 0.9$ [0.9–1.0]), and accelerating (cluster 3: $GRR_6 = 1.2$ [1.1–1.3]).

Table 2 presents the clinical and radiological features of meningiomas according to the cluster type at t_0 . The age at diagnosis and tumour volume (V_0) significantly increased from cluster 4 to 1 (age: 56.9 and 64.7 years, respectively; tumour volume: 0.34 and 1.43 cm³, respectively). The proportion of patients who underwent cranial radiotherapy before the diagnosis of meningioma significantly increased from cluster 1 to 4 (3.4% and 26.3%, respectively). There were no significant associations between FLAIR hyperintensity, calcifications, oedema, or AIMSS risk score with cluster (Table S5, Supplementary Materials, Section IV). We observed a significant increase in the proportion of treated meningiomas from cluster 1 to 4 (3.4% and 68.4%, respectively), although there were no significant differences in the delay to treatment or tumour volume at treatment. Among the operated meningiomas, the proportion of WHO grade II tumours significantly increased from cluster 1 to 4 (0% and 64%, respectively).

At the end of the follow-up, 264 meningiomas (79%) remained in the same cluster. The remaining 69 tumours moved to a cluster with a lower growth rate, consistent with the Gompertz law (Table 2 and Figures S11 and S12 in Supplementary Materials, Section IV).

DISCUSSION

Meningioma growth rate was better fitted by the Gompertz and, to a lesser extent, power model compared to the linear and exponential models. To our knowledge, the present study is the largest series of the natural history of meningiomas.

The Gompertz model suggests progressive energy deprivation of cells in deep tissue layers with tumour growth,¹⁰ which is expressed mathematically as an exponential decrease in the intrinsic growth rate over time. The power model suggests that tumour growth is proportional to the power of the volume (V^γ , where $0 < \gamma < 1$); proliferating tissue, as a subset of the 3D space, would have a dimension of 3γ .⁷ This represents a simplified version of the Von Bertalanffy model,¹⁹ which was not used because of the large number of model parameters (4). Notably, in our series, the mean γ was $0.73 (\pm 0.03)$ (data not shown); this is close to Kleiber's law,⁷ according to which an exponent γ of $3/4$ would provide the most efficient energy consumption. However, regardless of γ , there is no slow growth or plateau phase in the power model, which contradicts the findings of both the present (Figure 1, IDs 12 and 53 and figure S12, supplementary materials) and previous studies.^{12,20,21} These results, and those regarding the goodness-of-fit criteria, suggest that the Gompertz model is the most appropriate to describe the volumetric evolution of meningiomas.

The Gompertz model has been used to analyse meningioma growth by previous studies^{5,12,22} that differed in several key respects from our study. The present study had a larger sample size than previous studies, which is advantageous with respect to modelling, statistical comparison of models, population representativeness, and the reproducibility of the results. Furthermore, the population approach is superior in terms of the robustness and accuracy of data fitting compared to the individual, non-linear regression approach used by previous studies.^{5,12,22} Finally, we calculated the AIC and BIC, which are comprehensive criteria that consider model complexity, rather than R^2 , which has questionable ability to quantify the accuracy of non-linear models.

Based on the $RGR_{\pm 6}$ and GRR_6 values, hierarchical clustering was used to classify tumour growth into four phases at diagnosis: slow (8.7%), linear (63.7%), accelerating (21.9%), and fast-accelerating (5.7%). Behbahani et al.²⁰ identified several growth patterns without considering the possibility that they may be the phases of the same Gompertz' law. Interestingly, a greater proportion of patients exhibited a slow growth pattern in Behbahani et al.²⁰ and Nakasu et al.²¹ compared to our study, suggesting selection bias in favour of small or slow-growing tumours. Notably, we excluded 4 of 337 (1.2%) meningiomas because of a spontaneous decrease in tumour size over time, which is a smaller proportion than reported previously (2.5–5.6%^{23,20}); this might be because we used a strict criterion for the change in tumour size and excluded patients receiving macroprogestative treatment at diagnosis.

Patient age and tumour volume at diagnosis were significantly associated with growth tumour patterns in this study, with pseudo-exponential clusters observed in younger patients and those with small tumours. This is in line with the Gompertz law, as clusters 3 and 4 correspond to an earlier stage in the natural history of the tumour. Previous studies reported conflicting results regarding age as a factor associated with tumour growth^{15,20,24–26} and volume.^{20,23,24,27,28} Furthermore, an increasing proportion of patients underwent cranial radiotherapy before a diagnosis of meningioma from cluster 4 to 1 (26.3% of tumours in cluster 4), consistent with previous findings that radiotherapy-induced meningiomas are more aggressive than those not associated with radiotherapy.^{23,29} Among our operated patients, there was a significantly higher proportion of WHO grade II meningiomas in clusters 3 and 4, consistent with the finding of exponential growth in these tumours.²¹ Taken together, these findings support our clustering analysis and modelling of tumour growth using Gompertz law.

Meningioma growth is classically described in terms of the mean linear (cm^3/year) or exponential growth rate ($\%/ \text{year}$ or TDT), based on the first and last scans of the observation period, and extrapolated as a constant feature of the tumour. In the present study, over a mean follow-up of 56.5 months, 21% of the tumours moved from one cluster to another. Indeed, the usefulness of categorising meningiomas as “slow” or “fast” growing based on the mean tumour growth rate is unclear. In addition, the threshold used to categorize tumours varies between studies, which makes identification of risk factors of rapid growth challenging. Previously, risk factors of tumour growth were identified by Cox models of radiological progression-free survival^{23,24,30,31} using different definitions of progression, or by multivariate models based on the mean growth rate.^{4,15,20,23,25,32} Therefore, we investigated whether any clinical or

radiological factors correlated with the four growth patterns identified at diagnosis. Except for initial tumour volume, age at diagnosis, and previous cranial radiotherapy, there were no associations of FLAIR hyperintense signals, calcifications, or surrounding oedema with the patterns. This contradicts the classical finding that rapidly growing meningiomas often have FLAIR hyperintense signals and surrounding oedema, whereas calcified meningiomas show no or slow growth.^{4,23,25} However, there is no consensus on the predictive value of these radiological characteristics. To our knowledge, none of the risk scores based on these factors^{15,25} have been validated in prospective independent cohort studies. The discrepant results among studies may be due to the radiological features being analysed qualitatively, such that they may be subject to interobserver variability. Future cohort studies should use radiomics to provide further information.

To test for selection bias, we evaluated the characteristics of the excluded tumours with fewer than three observation time points. On the one hand, we observed a trend to quicker AGR and TGR and significantly shorter TDT in the excluded tumours, but on the other hand, a smaller proportion of excluded tumours had been treated, indicating that selection bias was not introduced by eliminating meningiomas with only two imaging scans. The main limitation of this study is the measurement of volume. Although we used semiautomated segmentation software specifically designed for meningioma segmentation - which undoubtedly makes volume measurement more accurate compared with studies using simple 2D planar measurements, as shown by Huang et al.³³ - and although neurosurgeons have validated, some measurements may remain inaccurate. In addition, the exploratory study of intra- and inter-observer reproducibility showed excellent agreement between measurements, with an average error of 16%, which is very close to the 15% usually reported in the literature²⁵ (see supplementary material). The accuracy of volumetry depends on the characteristics of both the radiological examination and tumour. To account for uncertainty due to imprecise measurements, we included measurement error in the mathematical models.

CONCLUSION

Between the four growth laws compared in this study, the Gompertz model gave the best results, provided that other models could be tested. This means that the growth rate of meningioma might be not constant over time. This observation calls into question the dichotomization of meningiomas as more or less aggressive tumours according to the average growth rate

computed over the whole observation period and shows how difficult it is to define radiological predictive factors for “rapid growth”. The clinical and pragmatic conclusion is that the management strategy should be discussed according to the growth phase in addition to the location, size, growth rate and patient’s comorbidities. We emphasize that the estimated parameters and associated growth rates of the real cohort could be used as a training data set for the classification of a newly diagnosed tumor. The main drawback is that we need at least 3 time points within a 12-month observation period for an acceptable estimate of the parameters of this new tumor. In particular, because there is no significant correlation between the cluster and the volume at diagnosis. Therefore, the main perspective of this work is to predict the cluster by enriching the data taking into account the imaging features at diagnosis.

DATA SHARING STATEMENT

Data collected for the study, including deidentified individual participant data, informed consent form, will be made available on demand for any purpose immediately following publication and indefinitely by writing to the corresponding author.

BIBLIOGRAPHY

- 1 Baldi I, Engelhardt J, Bonnet C, *et al.* Epidemiology of meningiomas. *Neurochirurgie* 2018; **64**: 5–14.
- 2 Pouchieu C, Gruber A, Berteaud E, *et al.* Increasing incidence of central nervous system (CNS) tumors (2000-2012): findings from a population based registry in Gironde (France). *BMC Cancer* 2018; **18**: 653.
- 3 Goldbrunner R, Minniti G, Preusser M, *et al.* EANO guidelines for the diagnosis and treatment of meningiomas. *Lancet Oncol* 2016; **17**: e383–91.
- 4 Islim AI, Mohan M, Moon RDC, *et al.* Incidental intracranial meningiomas: a systematic review and meta-analysis of prognostic factors and outcomes. *J Neurooncol* 2019; **142**: 211–21.
- 5 Huttner HB, Bergmann O, Salehpour M, *et al.* Meningioma growth dynamics assessed by radiocarbon retrospective birth dating. *EBioMedicine* 2018; **27**: 176–81.
- 6 Schwartz M. A biomathematical approach to clinical tumor growth. *Cancer* 1961; **14**: 1272–94.
- 7 Benzekry S, Lamont C, Beheshti A, *et al.* Classical mathematical models for description and prediction of experimental tumor growth. *PLoS Comput Biol* 2014; **10**: e1003800.
- 8 Gompertz B. On the nature of the function expressive of the law of human mortality, and on a new mode of determining the value of life contingencies. In a letter to Francis Baily, Esq. FRS &c. *Philos. Trans. R. Soc. Lond.* 1825; : (115):513-583.
- 9 Laird AK. DYNAMICS OF TUMOUR GROWTH: COMPARISON OF GROWTH RATES AND EXTRAPOLATION OF GROWTH CURVE TO ONE CELL. *Br J Cancer* 1965; **19**: 278–91.
- 10 Norton L. A Gompertzian model of human breast cancer growth. *Cancer Res* 1988;

48: 7067–71.

- 11 Pérez-García VM, Calvo GF, Bosque JJ, *et al.* Universal scaling laws rule explosive growth in human cancers. *Nat Phys* 2020; **16**: 1232–7.
- 12 Nakasu S, Nakasu Y, Fukami T, Jito J, Nozaki K. Growth curve analysis of asymptomatic and symptomatic meningiomas. *J Neurooncol* 2011; **102**: 303–10.
- 13 Ribba B, Holford NH, Magni P, *et al.* A review of mixed-effects models of tumor growth and effects of anticancer drug treatment used in population analysis. *CPT Pharmacomet Syst Pharmacol* 2014; **3**: e113.
- 14 Collin A, Copol C, Pianet V, *et al.* Spatial mechanistic modeling for prediction of the growth of asymptomatic meningiomas. *Comput Methods Programs Biomed* 2021; **199**: 105829.
- 15 Lee EJ, Kim JH, Park ES, *et al.* A novel weighted scoring system for estimating the risk of rapid growth in untreated intracranial meningiomas. *J Neurosurg* 2017; **127**: 971–80.
- 16 Burnham, K. P.; Anderson, D. R. Model Selection and Multimodel Inference: A practical information-theoretic approach, Springer-Verlag, 2002.
- 17 Burnham KP, Anderson DR. Model selection: understanding AIC and multimodel inference, with contrasts to BIC. *Sociol Methods Res* 2004; **33**: 261–304.
- 18 Shmueli G. To Explain or to Predict? *Stat Sci* 2010; **25**: 289–310.
- 19 Von Bertalanffy L. Quantitative laws in metabolism and growth. *Q Rev Biol* 1957; **32**: 217–31.
- 20 Behbahani M, Skeie GO, Eide GE, Hausken A, Lund-Johansen M, Skeie BS. A prospective study of the natural history of incidental meningioma—Hold your horses! *Neuro-Oncol Pract* 2019; **6**: 438–50.
- 21 Nakasu S, Fukami T, Nakajima M, Watanabe K, Ichikawa M, Matsuda M. Growth pattern changes of meningiomas: long-term analysis. *Neurosurgery* 2005; **56**: 946–55; discussion 946–955.
- 22 Ehresman JS, Mampre D, Rogers D, Olivi A, Quinones-Hinojosa A, Chaichana KL. Volumetric tumor growth rates of meningiomas involving the intracranial venous sinuses. *Acta Neurochir (Wien)* 2018; **160**: 1531–8.
- 23 Thomann P, Häni L, Vulcu S, *et al.* Natural history of meningiomas: a serial volumetric analysis of 240 tumors. *J Neurosurg* 2022; **137**: 1639–49.
- 24 Oya S, Kim S-H, Sade B, Lee JH. The natural history of intracranial meningiomas. *J Neurosurg* 2011; **114**: 1250–6.
- 25 Islim AI, Kolamunnage-Dona R, Mohan M, *et al.* A prognostic model to personalize monitoring regimes for patients with incidental asymptomatic meningiomas. *Neuro-Oncol* 2020; **22**: 278–89.
- 26 Islim AI, Ali A, Bagchi A, *et al.* Postoperative seizures in meningioma patients: improving patient selection for antiepileptic drug therapy. *J Neurooncol* 2018; **140**: 123–34.
- 27 Nakamura M, Roser F, Michel J, Jacobs C, Samii M. The natural history of incidental meningiomas. *Neurosurgery* 2003; **53**: 62–70; discussion 70–71.
- 28 Yano S, Kuratsu J, Kumamoto Brain Tumor Research Group. Indications for surgery in patients with asymptomatic meningiomas based on an extensive experience. *J Neurosurg* 2006; **105**: 538–43.
- 29 Gillespie CS, Islim AI, Taweel BA, *et al.* The growth rate and clinical outcomes of radiation induced meningioma undergoing treatment or active monitoring. *J Neurooncol* 2021; **153**: 239–49.
- 30 Delgado-López PD, Montalvo-Afonso A, Martín-Alonso J, *et al.* Volumetric growth rate of incidental asymptomatic meningiomas: a single-center prospective cohort study. *Acta Neurochir (Wien)* 2021; **163**: 1665–75.
- 31 Romani R, Ryan G, Benner C, Pollock J. Non-operative meningiomas: long-term

follow-up of 136 patients. *Acta Neurochir (Wien)* 2018; **160**: 1547–53.

32 Sughrue ME, Rutkowski MJ, Aranda D, Barani IJ, McDermott MW, Parsa AT. Treatment decision making based on the published natural history and growth rate of small meningiomas. *J Neurosurg* 2010; **113**: 1036–42.

33 Huang RY, Unadkat P, Bi WL, *et al.* Response assessment of meningioma: 1D, 2D, and volumetric criteria for treatment response and tumor progression. *Neuro-Oncol* 2019; **21**: 234–41.

FIGURES AND TABLES

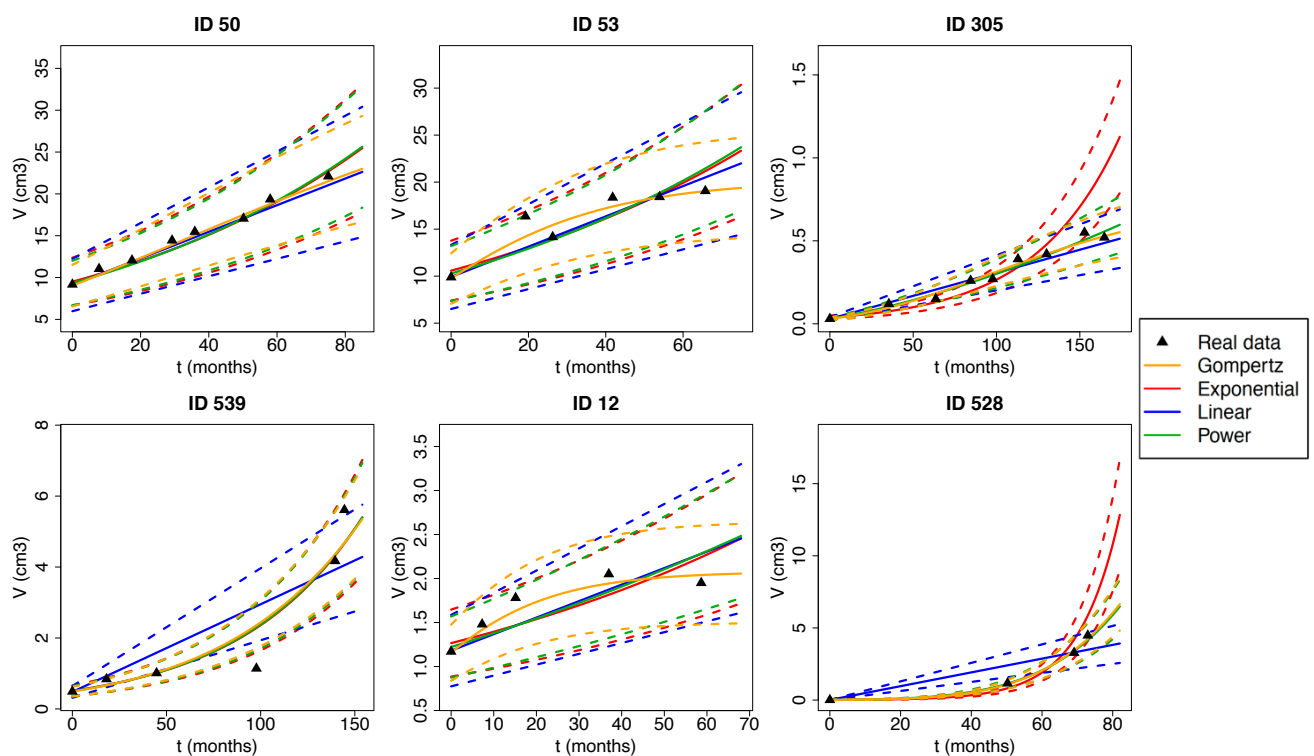


Figure 1. Representative tumour growth modelling using the four models. *The exponential model did not fit the data for tumours #305 and #528 while the linear one did not fit the data #539. Tumours #50 and #53 had similar initial volumes (9.2 and 9.9 cm³, respectively) at the first imaging session, and a similar follow-up duration, but the growth patterns differed over time. For tumour #53, only the Gompertz model fitted the data well. For tumour #50, the four models showed similar performance. Tumour #12 had similar dynamics to tumour #53 despite a much smaller initial volume; only the Gompertz model fitted the data well.*

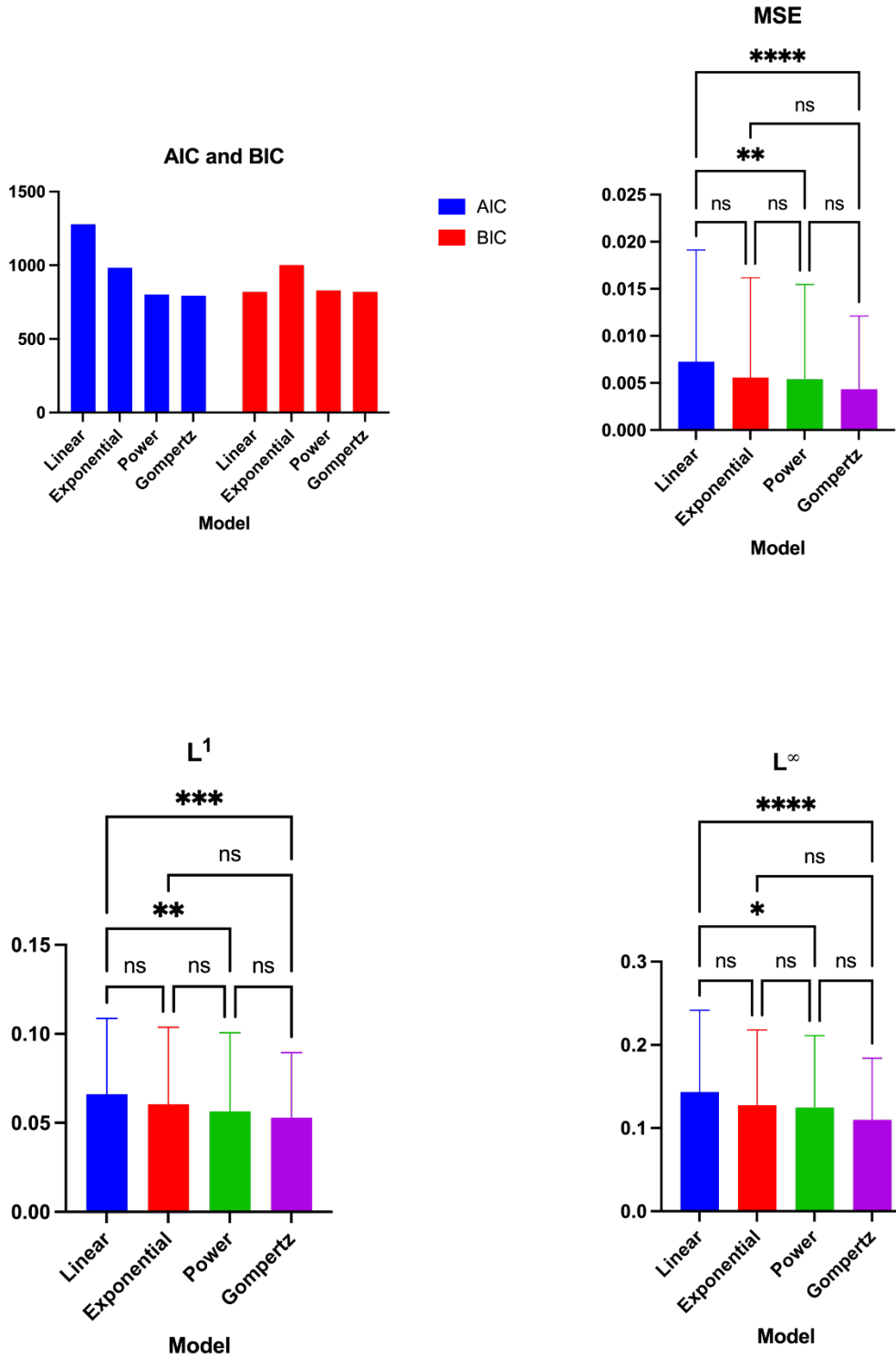


Figure 2. Fit performances of the four growth models based on the AIC, BIC, L^1 and L^∞ norms, and MSE values. Errors are displayed as bar charts (median and interquartile range) with vertical bars (*: $p < 0.05$; **: $p < 0.01$; ***: $p < 0.001$; ****: $p < 0.0001$; ns: not significant, according to the Kruskal-Wallis test). The AIC and BIC are used to select the model. The optimisation algorithm minimises the MSE. The L^∞ and L^1 errors are given as they are informative data (L^∞ indicates the worst error, and L^1 gives an idea of the percentage error).

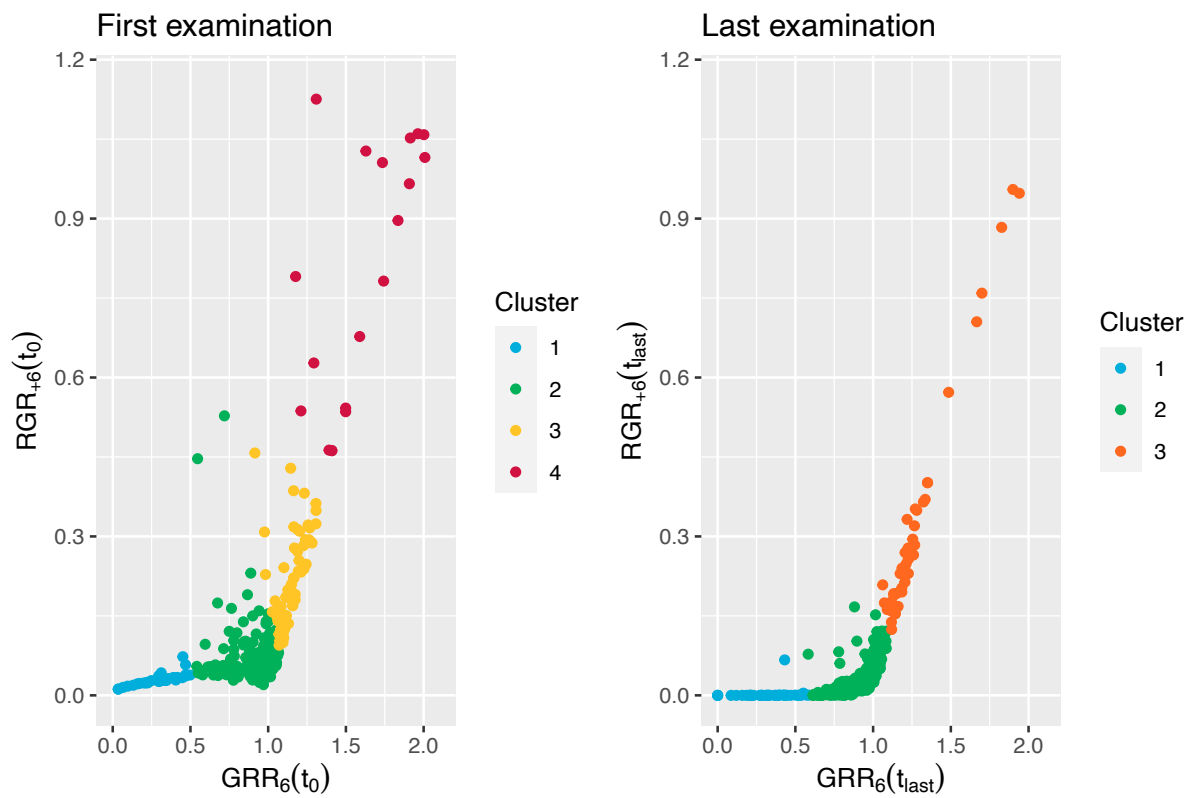















Figure 3. Results of hierarchical clustering analysis.

PATIENTS		N = 294
Sex ratio (F/M)		8•8
Age at diagnosis of the first meningioma		58•2 ± 13•3
Hormonal treatment at diagnosis*		13 (4•4%)
Prior hormonal therapy		40 (13•6%)
Prior cranial radiotherapy		10 (3•4%)
Meningiomatosis		61 (20•7%)
MENINGIOMAS		N = 333
Follow-up (months)		56•5 ± 39•5
Number of images		4 [4; 6]
Localization		
	<i>Convexity</i>	163 (48•6%)
	<i>Falx and tentorium</i>	75 (22•5%)
	<i>Skull base</i>	91 (27•3%)
	<i>Other</i>	5 (1•5%)
Radiological features		
	<i>FLAIR: hypersignal</i>	121 (36•3%)
	<i>Calcifications</i>	97 (29•1%)
	<i>Edema</i>	28 (8•4%)
Volume at first imaging (V_0) (cm ³)		1•3 [0•4; 3•4]
Volume at last imaging (V_{last}) (cm ³)		2•2 [0•8; 5•7]
AIMSS risk score		
	<i>Low</i>	98 (29•3%)
	<i>Intermediate</i>	208 (62•3%)
	<i>High</i>	27 (8•1%)
Mean growth-rate during the study period		
	<i>AGR (cm³/year)</i>	0•13 [0•02; 0•5]
	<i>TGR (%/year)</i>	9•5 [3•4; 22•7]
	<i>TDT (years)</i>	4•9 [1•6; 10•1]
Treatment		108 (32•4%)
	<i>Radiotherapy</i>	19 (5•7%)
	<i>Stereotactic radiotherapy</i>	18 (5•4%)
	<i>Surgery</i>	71 (21•3%)
	<i>Delay before treatment (months)</i>	51•3 ± 37•4
	<i>Volume at treatment (cm³)</i>	4•7 [2•8; 7•6]
Histology (operated tumors only)		N = 71
	<i>WHO grade I</i>	54 (76%)
	<i>WHO grade II</i>	17 (24%)

*excluded: cyproterone acetate• nomegestrol acetate and chlormadinone acetate

Table 1. Clinical and radiological data

Cluster at t_0	Cluster 1		Cluster 2		Cluster 3			Cluster 4			p										
Features																					
N (%)	29 (8.7%)		212 (63.7%)		73 (21.9%)			19 (5.7%)													
RGR ₊₆ (%)	2.8 [2.3; 3.5]		6.6 [4.9; 8.5]		19.4 [14.3; 28.8]			79.1 [53.7; 102.8]													
GRR ₆	0.3 [0.2; 0.4]		1.0 [0.9; 1.0]		1.1 [1.1; 1.2]			1.6 [1.4; 1.9]													
Baseline features (t_0)																					
Sex ratio (F/M)	8.7		10.2		8.1			8.5			0.74*										
Age at diagnosis	64.7 [59.4; 68.4]		58.6 [50.1; 67.4]		52.2 [43.0; 66.0]			56.9 [45.6; 69.1]			<0.001*										
Hormonal treatment at diagnosis	3 (10.3%)		7 (3.3%)		4 (5.5%)			0			0.44*										
Prior hormonal therapy	7 (24.1%)		27 (12.7%)		15 (20.6%)			0			0.64*										
Prior cranial radiotherapy	1 (3.4%)		5 (2.4%)		4 (5.5%)			5 (26.3%)			0.003*										
Meningiomatosis	10 (34.5%)		64 (30.2%)		17 (23.3%)			7 (36.8%)			0.42*										
V ₀ (cm ³)	1.43 [0.50; 3.03]		1.72 [0.58; 4.22]		0.63 [0.14; 2.04]			0.34 [0.08; 1.92]			<0.001*										
FLAIR hypersignal	14 (48.3%)		63 (29.7%)		33 (45.2%)			11 (57.9%)			0.077*										
Calcifications	4 (13.8%)		75 (35.4%)		15 (20.5%)			3 (15.8%)			0.22*										
Edema	1 (3.4%)		22 (10.4%)		4 (5.5%)			1 (5.3%)			0.56*										
End of follow-up features (t_{last})																					
Follow-up (months)	52.5 [34.9; 78.9]		48.9 [24.3; 81.6]		48.8 [21.8; 85.5]			22.3 [15.7; 54.8]			0.062*										
Number of observations	4 [4; 6]		4 [4; 6]		4 [4; 6]			3 [3; 4]			0.087*										
Treatment	1 (3.4%)		56 (26.4%)		38 (52.1%)			13 (68.4%)			<0.001*										
<i>Radiotherapy</i>	0		12		7			0													
<i>SRS</i>	0		8		8			2													
<i>Surgery</i>	1		36		23			11													
Delay to treatment (months)	109.5		39.2 [17.5; 83.8]		42.6 [18.2; 77.7]			18.2 [13.7; 59.3]			0.24*										
Volume at treatment (cm ³)	1.8		5.3 [3.1; 11.3]		4.0 [2.5; 5.7]			6.6 [4.6; 17.2]			0.93*										
Histology. N =	1		36		23			11													
WHO grade I	1 (100%)		31 (86%)		18 (78%)			4 (36%)			0.004*										
WHO grade II	0		5 (14%)		5 (22%)			7 (64%)													
Cluster at t_{last}																					
N (%)	29 (100%)		10 (4.7%)		202 (95%)		1 (1.4%)			39 (53%)		33 (45%)		1 (5.3%)			5 (26%)		13 (68%)		

*: Spearman's correlation

** : Kruskal-Wallis' test

Table 2: Baseline and end of follow-up features of the meningiomas categorized according to the hierarchical clustering at T0.

SUPPLEMENTARY MATERIALS

I. Exploratory study of the accuracy of volumetric measurements

The first step was the selection of the tumours to be re-segmented. We selected 10 tumours with 3 observations, *i.e.* 30 images to re-segment. Then we looked at the volume/time curves and selected 3 tumours for which the volume variation could indicate a volume error, 4 tumours for which the measurement seemed correct (small and large volume tumours), and then we selected 3 tumours at random. This procedure is certainly penalising as it tends to overestimate the inaccuracy.

We investigated the reliability of the measurements (intra- and inter-observer). The same author (HL) re-segmented the tumours (intra-individual correlation), and a secondary author (JE) also re-segmented the tumours (inter-observer correlation). The reliability of the measures was estimated by the intraclass correlation coefficient (ICC) in a two-factor random effects model for a single assessment. The ICC was equal to 0.984, 95% CI (0.971; 0.991), $p < 0.001$, indicating excellent measurement reliability.

Secondly, we tried to estimate the precision of the measurement. We have considered that the mean of all the measurements will be closer to the ground truth. Using this, we computed the relative mean absolute error with the new volumes obtained. Thus, for each meningioma j , we have computed:

$$\text{Err}_j = \frac{1}{3} \sum_{i=1}^3 \frac{|x_i - \bar{x}|}{|\bar{x}|}.$$

Using the global average of everything we obtained an estimated error of 14.6%, 95% CI (5.8; 23.5) which is very close to the one estimated by the mixed-effect approach, and the data published in the literature. This reinforces our opinion about the robustness of the method used.

II. Definitions and formulas

For each individual meningioma j , we denoted by $(V_k^j)_{0 \leq k < N_{\text{MRI}}^j}$, the N_{MRI}^j volumes obtained at time $(t_k^j)_{0 \leq k < N_{\text{MRI}}^j}$, where N_{MRI}^j is the number of segmented MRI scans.

The relative L^1 , L^∞ and the MSE (mean squared error) errors between the estimated and real volumes are written as follows:

$$\begin{aligned} \mathcal{E}_{L^1}^j &= \frac{1}{N_{\text{MRI}}^j} \sum_{k=1}^{N_{\text{MRI}}^j} \frac{|\hat{V}^j(t_k^j) - V_k^j|}{V_k^j}, \quad \mathcal{E}_{L^\infty}^j = \max_{1 \leq j \leq N_{\text{MRI}}^j} \frac{|\hat{V}^j(t_k^j) - V_k^j|}{V_k^j} \text{ and} \\ \text{MSE}^j &= \frac{1}{N_{\text{MRI}}^j} \sum_{k=1}^{N_{\text{MRI}}^j} \frac{(\hat{V}^j(t_k^j) - V_k^j)^2}{(V_k^j)^2}. \end{aligned} \quad (1)$$

III. Assessment of the parameter estimation of the Gompertz model for description and prediction of the growth of meningiomas using synthetic data

1- Comparison of two estimation approaches

Because the Gompertz model $V(t) = V_0 e^{\frac{\alpha}{\beta}(1-e^{-\beta t})}$ best described the population of meningiomas included in this study, we evaluated this model further. This model depends on three parameters: α , β and the initial volume

V_0 which must be estimated for each meningioma. In this appendix, two approaches were compared. The first one – the so-called individual one - considers each meningioma individually and estimates the parameters using the very classical optimization algorithm: the Levenberg-Marquardt algorithm [1], implemented in the R-package *marqLevAlg* [2]. The second approach is called the population approach. In this strategy, we used the mixed-effect approach [3] which consists in pooling all meningiomas and estimating a global distribution of the model parameters in the population.

In the second approach, the individual parameters α^j , β^j and γ^j , (where j denotes the individual) are assumed to be realizations of a random variable decomposed into two parts:

$$\log(\{\alpha, \beta\}^j) = \log(\{\alpha, \beta\}^{pop}) + \{\tilde{\alpha}, \tilde{\beta}\}^j, \text{logit}(\{\gamma\}^j) = \text{logit}(\{\gamma\}^{pop}) + \{\tilde{\gamma}\}^j, \quad (2)$$

where $\{\alpha, \beta, \gamma\}^{pop}$ corresponds to the fixed effects and $\{\tilde{\alpha}, \tilde{\beta}, \tilde{\gamma}\}^j$ corresponds to the random effects and have been assumed with mean zero.

Models also depend on the initial volume \hat{V}_0^j , which can be fixed as the volume computed from the first MRI scan V_0^j (which does not consider the uncertainty of the segmentation process). Therefore, we considered the \hat{V}_0^j of each meningioma to be a covariate of the estimated volume at the initial time:

$$\hat{V}_0^j = V_0^j(1 + e_0), \quad (3)$$

where e_0 follows a Gaussian law of mean zero and of standard deviation which is estimated.

For both approaches, we assumed that the measurement error for all volumes was proportional

$$V_k^j = \hat{V}^j(t_k^j)(1 + e), \text{ for all } 0 \leq k < N_E^j, \quad (4)$$

where \hat{V}^j corresponds to the estimated volume using the models and e the measurement error. In the second approach, we assumed that e followed a Gaussian law of mean zero and its standard deviation σ_e was estimated and used to define the 95% confidence interval given in the fits. We used the Stochastic Approximation Expectation-Maximization algorithm (SAEM), implemented in Monolix library [4].

To compare the two above approaches, N_c cohorts of N_m artificial meningiomas were created:

- (1) for each cohort, N_m sets of parameters $\theta^j = (V_0^j, \alpha^j, \beta^j)$ were generated according to the laws: $V_0 \sim \mathcal{N}(0.065, 1.56)$, $\log(\alpha) \sim \mathcal{N}(-4.21, 0.82)$ and $\log(\beta) \sim \mathcal{N}(-4.21, 0.82)$,
- (2) several (from 3 to 10) time data about 6 months apart were randomly selected,
- (3) and noise from 0% to 5% was added (higher noise is considered below only in the population approach, since individual estimation regularly fails at higher noise).

The parameters of Gaussian laws, the number of time points and the spacing between them were chosen to produce synthetic databases similar to the real ones. The above two estimation strategies were then applied to these artificial meningiomas. The parameters thus estimated are denoted by $\hat{\theta}_j$. Fifty groups ($N_c = 50$) of 300 patients ($N_m = 300$) were generated to test the stability of our results using the population approach. The cohort size is a compromise between the size of the real data cohort (~350) and the computation times resulting from the very numerous tests required to validate our strategy, particularly because the individual estimation approach regularly failed.

For the three parameters, the estimated values of parameters $\hat{\theta}_j$ were compared to the real values θ_j using the mean absolute error $\text{MAE}^j = |\theta^j - \hat{\theta}^j|$. As shown in Fig. S2, the populational approach led to best results and had a higher robustness. The individual approach appeared to be very sensitive to the added noise and led to higher errors. Six illustrative meningiomas are shown in Fig. S3.

As the population approach provided the best results, we explored the robustness of this strategy after adding noise (0–15%). The maximum value was selected because it corresponds to the estimated error in our real cohort. Figure S4 shows the ability of the population approach to deal with high noise.

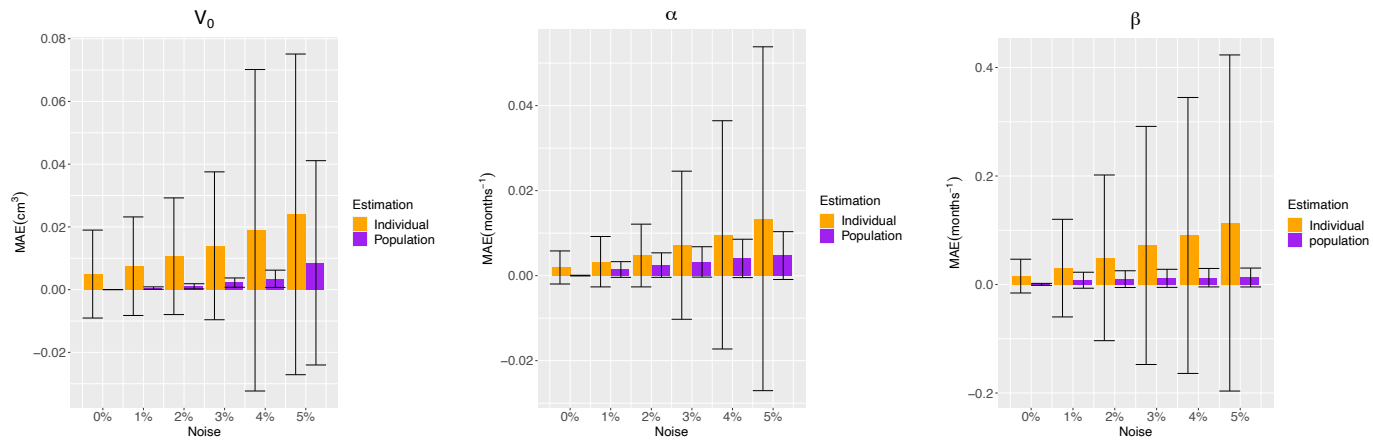


Figure S2. Estimation errors ($MAE^j = |\theta^j - \hat{\theta}^j|$) for the 3 parameters estimated using the 2 strategies. Orange: errors obtained with the individual approach, purple: with the population approach.

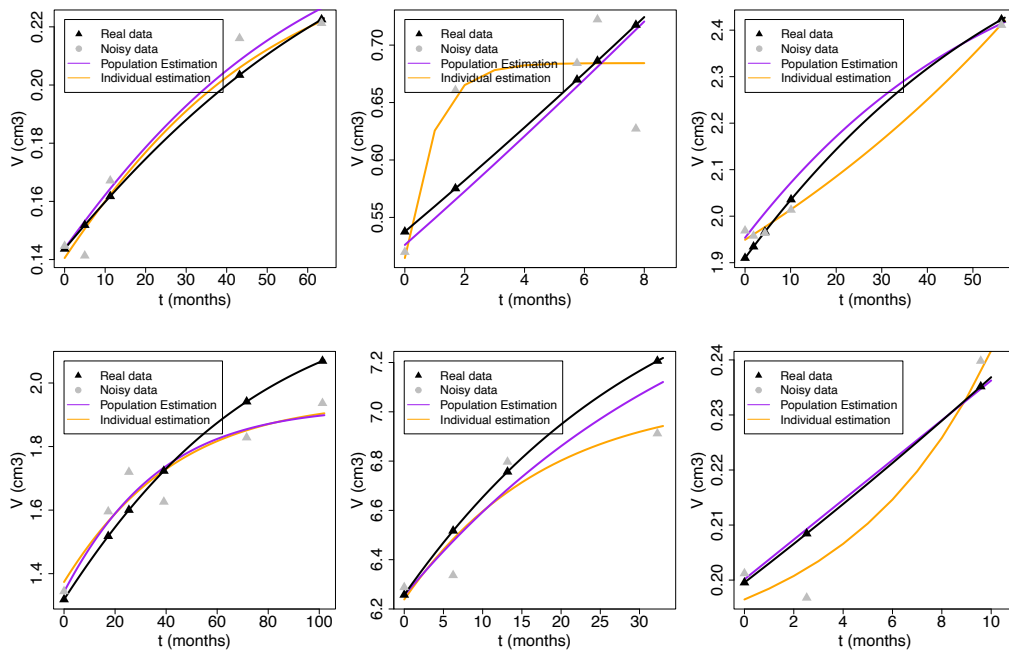


Figure S3. Six representative meningiomas. Black triangles and black curves: real data; grey triangles: noisy data (5%); purple curves: population estimations; orange curves: individual estimations.

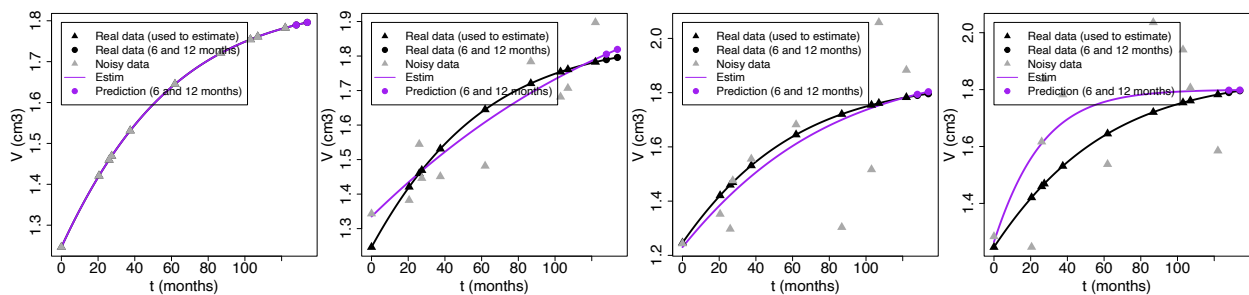


Figure S4. One representative synthetic meningioma. Real and predicted data are denoted by triangles and circles, respectively. Noisy data (left to right: 0%, 5%, 10%, and 15% noise) are indicated by grey triangles. Population estimations (purple) and predicted values (circle) are shown.

2- Classification of meningiomas

Percent increase in tumor volume - We classified meningiomas on the basis of the estimated percent increase in tumour volume. Thus, we calculated the relative growth rate (RGR) using the growth rate at a given time t , as follows:

$$\text{RGR}_{+X}(t) = \frac{V(t+X)-V(t)}{V(t)}, \text{RGR}_{-X} = \frac{V(t)-V(t-X)}{V(t)} \text{ and } \text{GRR}_X = \frac{\text{RGR}_{+X}}{\text{RGR}_{-X}}, \quad (5)$$

where X corresponds to the number of months.

If GRR_X^j is < 1 , the growth of the meningioma will be slowed. If GRR_X^j is 1, growth will be linear. If GRR_X^j is > 1 , the meningioma growth rate will be increased. When the Gompertz model is applied to calculate the tumour volume, RGR_{+X} and RGR_{-X} , and the growth rate ratio (GRR_X), decrease over time, which corresponds to a sigmoid curve.

We considered three X values (3, 6, and 12 months) and two times: t_0 (time of first imaging) and t_{last} (time of last imaging). The MAE was calculated and is shown in Fig. S5 for t_0 and Fig. S6 for t_{last} . The shorter the time X , the smaller the error. As can be seen from Figures S5 and S6, the errors for RGR_{+X} and RGR_{-X} were larger at t_0 than at t_{last} . In contrast, the errors for GRR_X were similar.

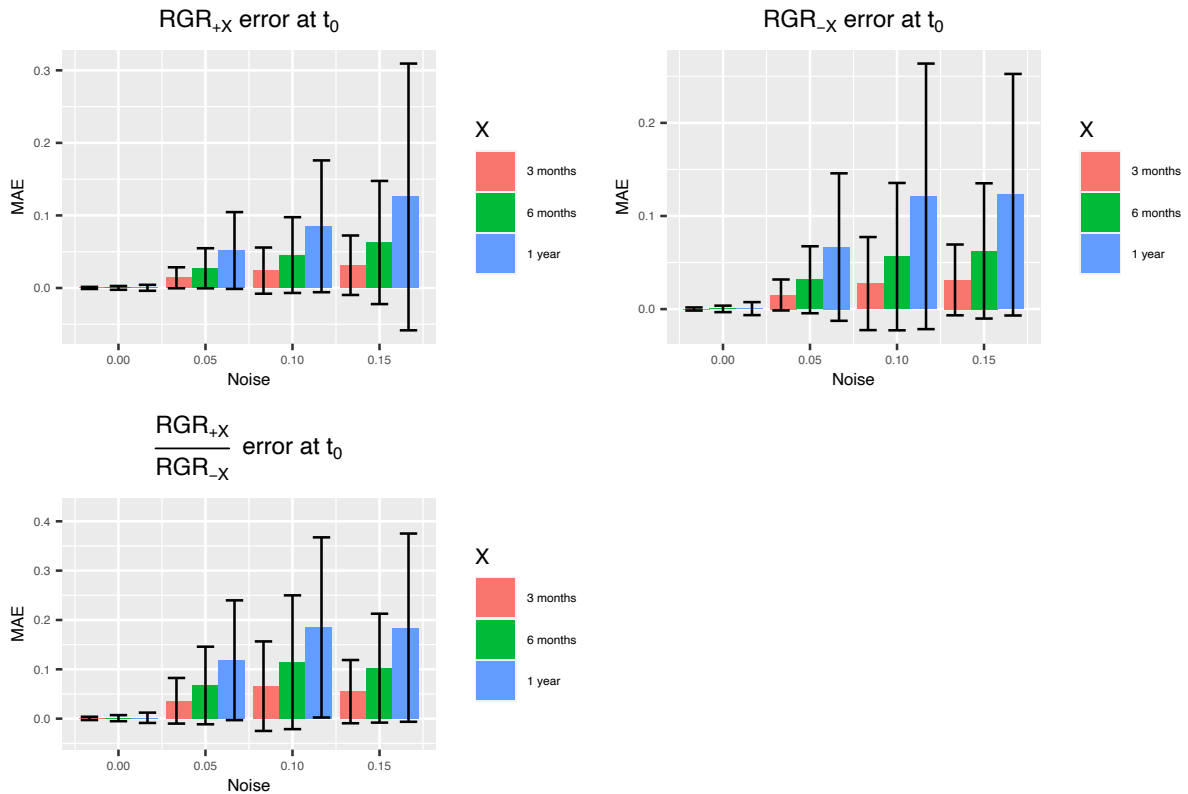


Figure S5. MAE of $\text{RGR}_{+X}(t_0)$, $\text{RGR}_{-X}(t_0)$ and $\text{GRR}_X(t_0)$ for $X = 3, 6$ and 12 months.

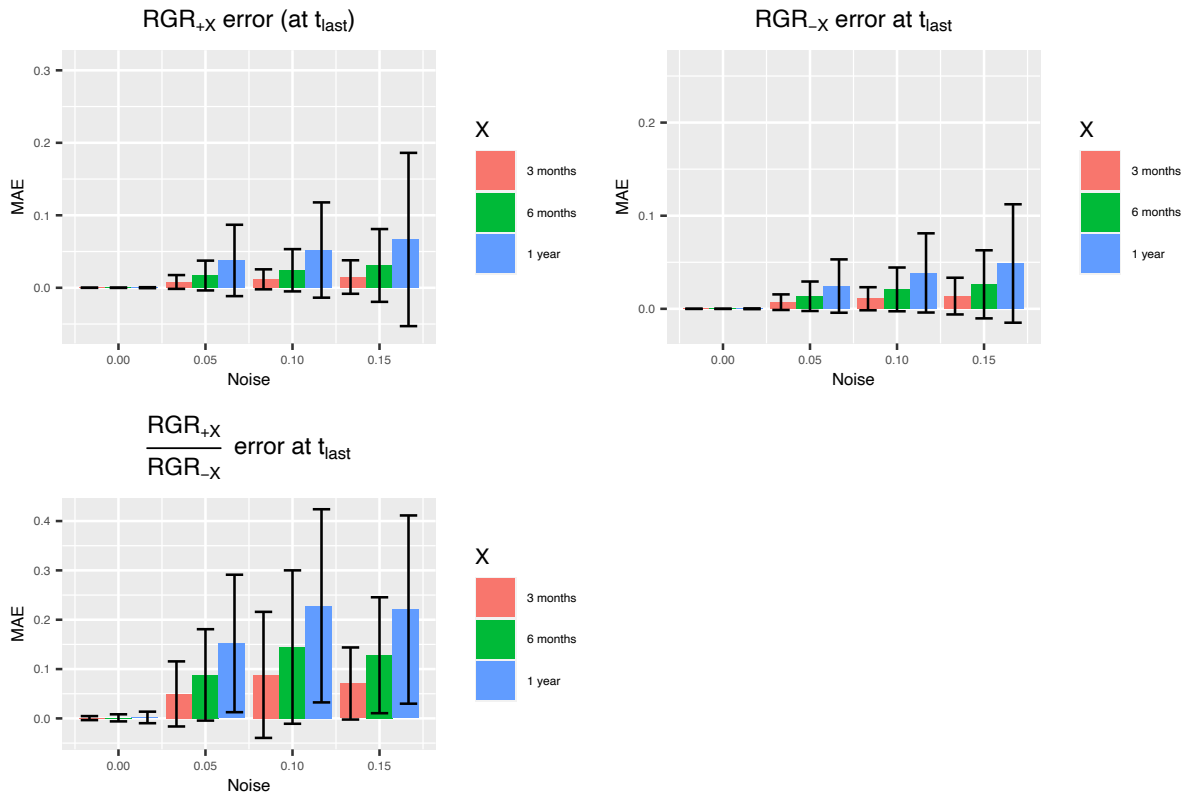


Figure S6. MAE of $RGR_{+X}(t_{last})$, $RGR_{-X}(t_{last})$ and $GRR_X(t_{last})$ for $X = 3, 6$ and 12 months.

Correlations of the observation time and number of observations: We focused on the GRR at 6 months because of acceptable errors in the first and last imaging scans. Moreover, the period was sufficiently long to detect a growth trend. We investigated the correlation between estimations and number of observations (Fig. S7). The same analysis was repeated according to the duration of the study period; the results are given in Fig. S8. No associations were observed between the parameters at t_0 or t_{last} .

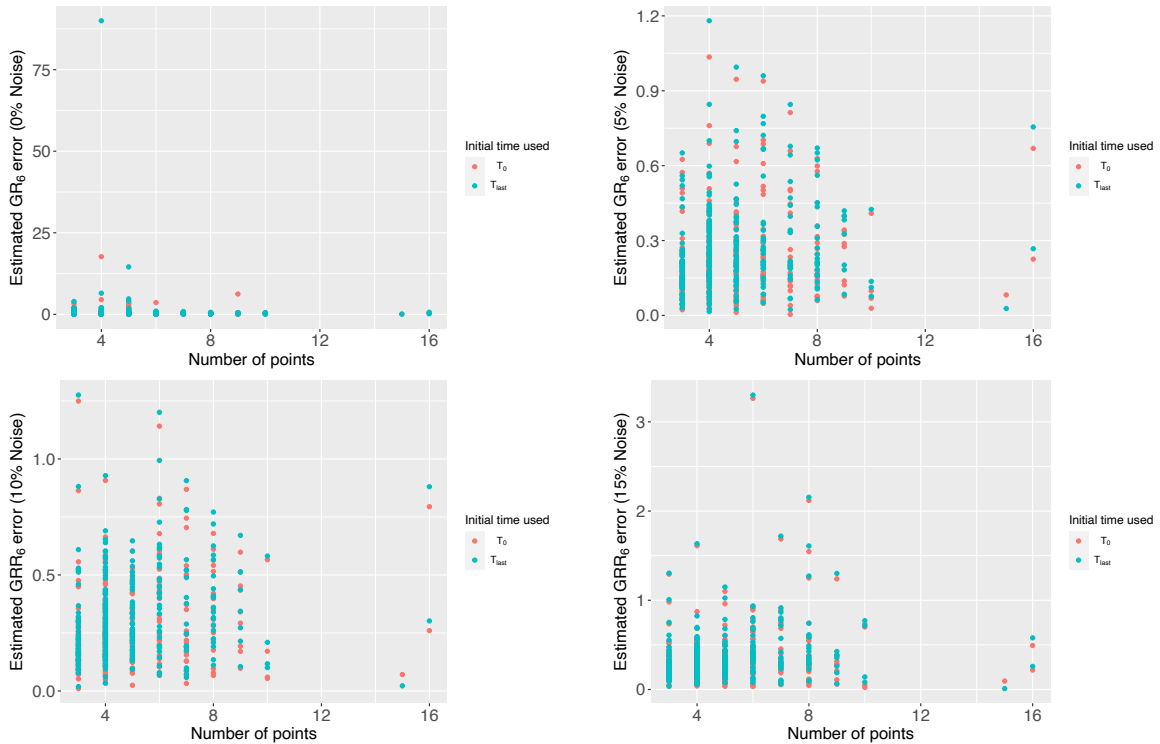


Figure S7. MAE of GRR_6 according to the number of observations.

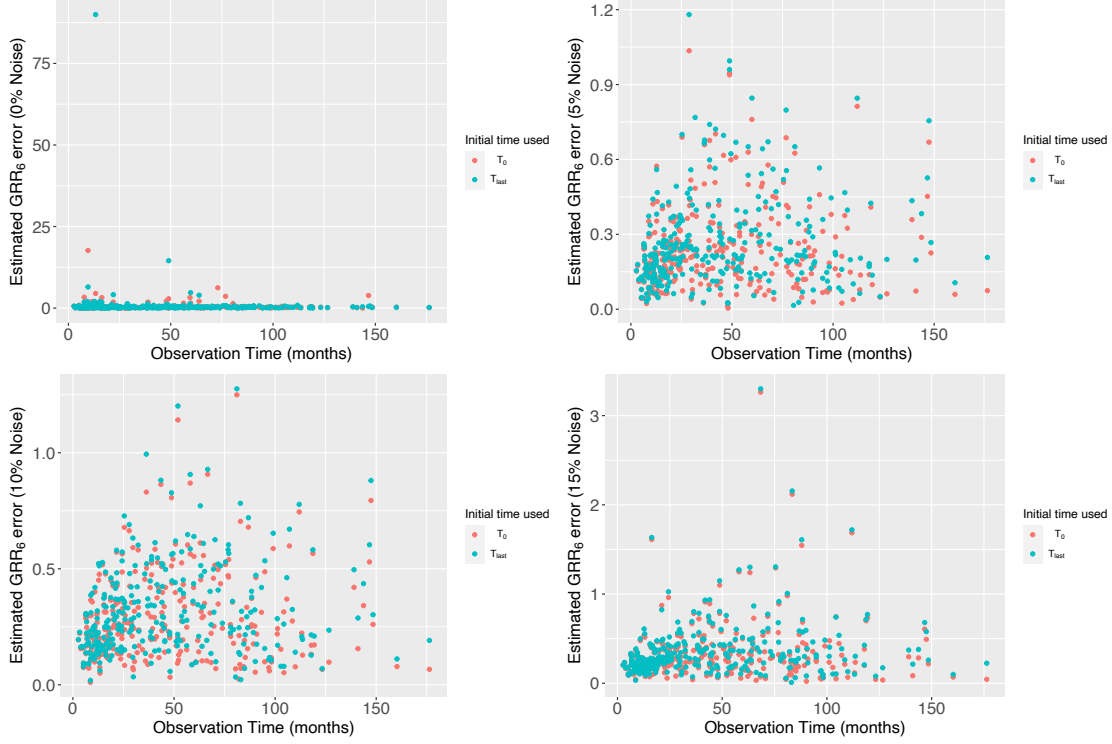


Figure S8. MAE of GRR_6 according to the observation time.

3. Robustness of the strategy

In practice, we can not know if the parameters to estimate follow a log-normal distribution. As it a strong assumption of mixed-effects strategy, we design two supplementary tests to explore the robustness of the method. We have generated 50 synthetic cohorts composed of 300 patients for which the parameters were taken following either a uniform distribution with $\alpha \sim U(0.01, 0.2)$ and $\beta \sim U(0.01, 0.2)$, or 3 subgroups log-normal distribution with $\alpha := (\alpha_1, \alpha_2, \alpha_3)$ $\beta := (\beta_1, \beta_2, \beta_3)$ and $Log(\alpha_1) \sim \mathcal{N}(0.03, 0.07)$, $Log(\alpha_2) \sim \mathcal{N}(0.2, 0.1)$, $Log(\alpha_3) \sim \mathcal{N}(0.35, 0.05)$, $Log(\beta_1) \sim \mathcal{N}(0.03, 0.07)$, $Log(\beta_2) \sim \mathcal{N}(0.2, 0.1)$, $Log(\beta_3) \sim \mathcal{N}(0.4, 0.1)$. We have then compared the results obtained with the ones where the synthetic parameters were chosen according a log-normal distribution. The exactly same approach was computed on these cohorts and we have decided to focus on the worst case, when 15% noise was added to the data. One can see that the results given in Table S1 are quite close and still acceptable for t_{last} , even if the assumption done in the mixed-effect approach (log-normal distribution of the parameters) deteriorate the results. As for the results at t_0 , the differences are more important and we advise using them carefully.

Table S1. Mean of MAE of the parameters and RGR estimations according to the parameters distribution chosen initially.

Distribution	Log-normal (reference)	Uniform	Log-normal (3 subgroups)
β	0.023 ± 0.029	0.027 ± 0.034	0.16 ± 0.16
α	0.011 ± 0.015	0.025 ± 0.026	0.08 ± 0.07
RGR ₊₆ at t_0	0.064 ± 0.098	0.18 ± 0.20	0.276 ± 0.29
RGR ₊₆ at t_{last}	0.033 ± 0.06	0.049 ± 0.072	0.04 ± 0.12
RGR ₋₆ at t_0	0.062 ± 0.083	0.11 ± 0.10	0.256 ± 0.30
RGR ₋₆ at t_{last}	0.027 ± 0.04	0.030 ± 0.033	0.030 ± 0.05
RGR at t_0	0.10 ± 0.11	0.15 ± 0.15	0.33 ± 0.32
RGR at t_{last}	0.13 ± 0.13	0.15 ± 0.14	0.32 ± 0.33

IV. Description of the cohort and analysis of tumour growth using the Gompertz model: supplementary figure and tables

Figure S9 shows the study flow chart.

Figure S10 shows the global growth dynamics of the meningiomas in the cohort.

Figure S11 shows that the GRR_6 at the last and first scans were significantly correlated ($p < 10^{-14}$). The colour inside the circle corresponds to the cluster based on the first scan and the colour outside the circle corresponds to the cluster based on the last scan. In total, 21% of the meningiomas changed cluster between t_0 and t_{last} .

Figure S12 presents two representative patients who exhibited a change in cluster between the first and the last follow-up.

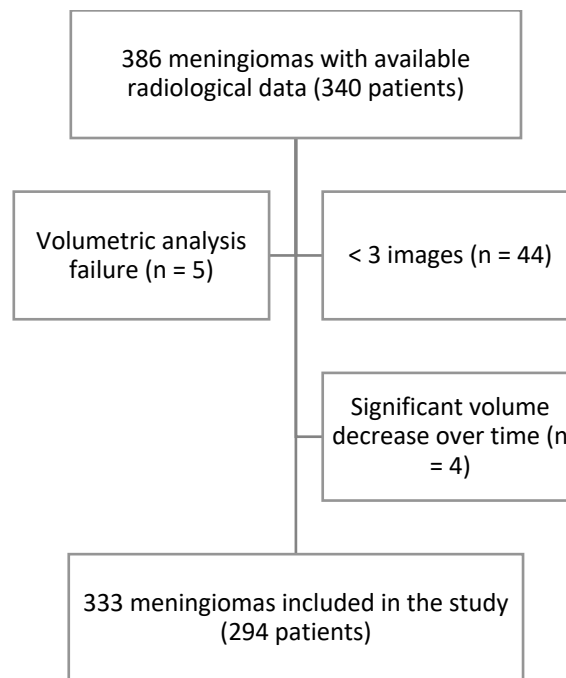


Figure S9. Study flow chart

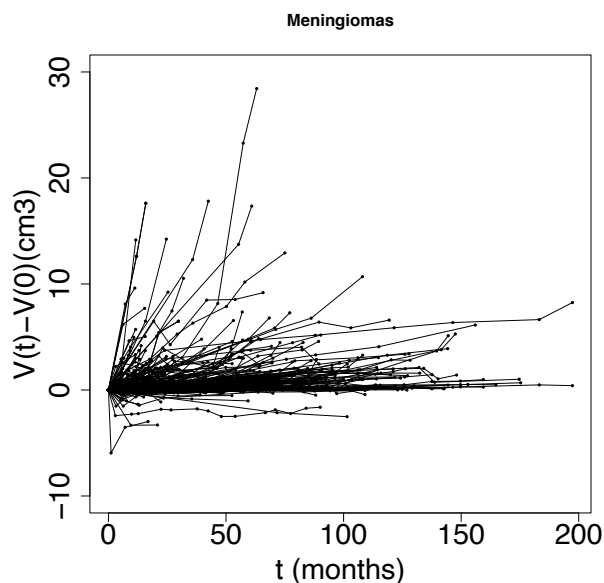


Figure S10. Spider plot representing the dynamic of the meningiomas in the cohort.

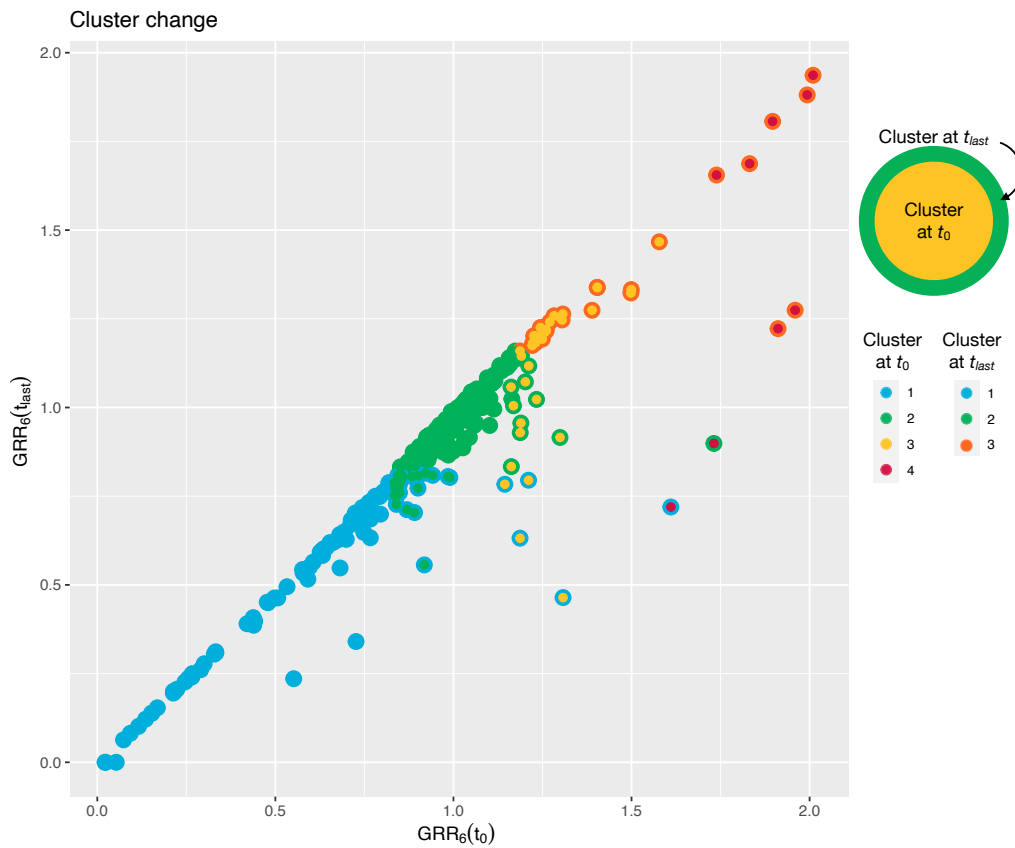


Figure S11. GRR_6 at the last and first examinations for the entire cohort. The colours inside and outside the circle correspond to the clusters based on the first and last scan, respectively.

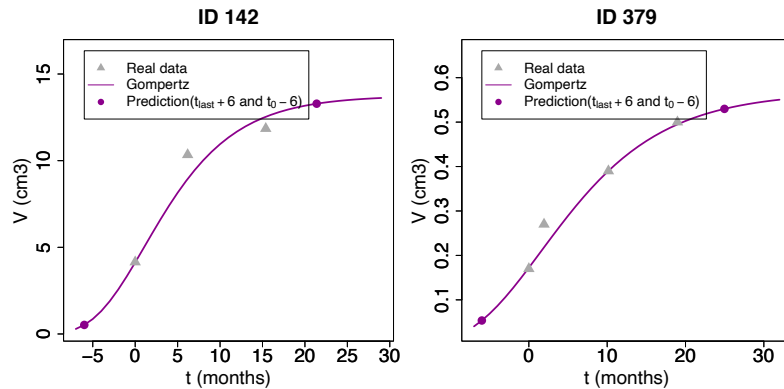


Figure S12. Representative tumours with different clusters between t_0 and t_{last} .
Left: cluster 4 to 1. Right: cluster 3 to 1.

Table S2 shows meningioma location according to the ICOM classification. Table S3 presents the clinical and radiological data for tumours with fewer than and at least three MRI scans. Table S4 shows the goodness-of-fit of the four models. Table S5 presents the correlation between the AIMSS risk score and cluster.

Table S2. Distribution of the location of the meningiomas according to the ICOM classification [5].

Localization	N	Frequency
Anterior fossa / NOS	9	2.7%
Anterior fossa / olfactory groove	2	0.6%
Anterior fossa / planum	19	5.7%
Anterior fossa / tuberculum sellae	16	4.8%
Sphenoid wing / lateral	22	6.6%
Sphenoid wing / medial	23	6.9%
Convexity / anterior	55	16.5%
Convexity / NOS	4	1.2%
Convexity / posterior	52	15.6%
Parasagittal / anterior	15	4.5%
Parasagittal / posterior	21	6.3%
Parafalcorial / anterior	15	4.5%
Parafalcorial / posterior	44	13.2%
Tentorium / infratentorial	9	2.7%
Tentorium / supratentorial	7	2.1%
Posterior fossa / squamous occipital	15	4.5%
Spinal	1	0.3%
Optic nerve	1	0.3%
Other	1	0.3%

Table S3. Radiological data and tumour treatments according to the number of MRI scans.

	Imaging ≥ 3 (n = 333)	Imaging < 3 (n = 44)	p
Follow-up (months)	48.4 [23.4; 78.5]	8.3 [6.0; 11.9]	< 0.001
FLAIR: hypersignal	121 (36.3%)	12 (27.3%)	0.24
Calcifications	97 (29.1%)	12 (27.3%)	0.80
Edema	28 (8.4%)	6 (13.6%)	0.26
Volume at first imaging (V_0) (cm^3)	1.3 [0.4; 3.4]	3.1 [0.4; 4.7]	0.10
Volume at last imaging (V_{final}) (cm^3)	2.2 [0.8; 5.7]	3.6 [0.5; 6.5]	0.80
AGR (cm^3/year)	0.1 [0.02; 0.5]	0.1 [-0.03; 0.8]	0.47
TGR (%/year)	9.4 [3.4; 22.7]	13.0 [-2.1; 38.7]	0.91
Tumor doubling time TDT (years)	4.9 [1.6; 10.1]	2.0 [-1.1; 5.3]	0.002
Treatment	108 (32.4%)	6 (13.6%)	0.02
<i>Radiotherapy</i>	19 (5.7%)	0	
<i>Stereotactic radiotherapy</i>	18 (5.4%)	1 (2.3%)	
<i>Surgery</i>	71 (21.3%)	5 (11.4%)	
Delay before treatment (months)	38.4 [17.5; 81.6]	26.1 [8.7; 44.5]	0.09
Volume at treatment (cm^3)	4.7 [2.8; 7.6]	4.7 [0.9; 7.9]	0.58

Table S4. Goodness-of-fit of the four models

Model	AIC	BIC	$\sum_j MSE^j$	$\sum_j \epsilon_{t_1}^j$	$\sum_j \epsilon_{t_\infty}^j$
Linear	1278.70	819.84	0.0073 [0.0032; 0.019]	0.066 [0.045; 0.11]	0.14 [0.091; 0.24]
Exponential	982.60	1001.64	0.0056 [0.0022; 0.016]	0.060 [0.038; 0.10]	0.13 [0.077; 0.22]
Power	801.84	828.84	0.0054 [0.0021; 0.015]	0.056 [0.035; 0.10]	0.12 [0.076; 0.18]
Gompertz	793.18	819.50	0.0043 [0.0019; 0.012]	0.053 [0.036; 0.089]	0.11 [0.072; 0.18]

Table S5. Results of crosstab analysis of clusters at T₀ and the AIMSS risk score.

AIMSS risk score	Cluster at T ₀				
	1	2	3	4	Total
Low	5	68	19	6	98
Intermediate	22	125	50	11	208
High	2	19	4	2	27
Total	29	212	73	19	333

There were no significant correlations (Spearman's Rho = -0.02; p = 0.73). Concordant and discordant classes are in green and red, respectively.

BIBLIOGRAPHY

- [1] J. J. Moré, "The Levenberg-Marquardt algorithm : implementation and theory," *Numerical analysis*, pp. 105-116, 1978.
- [2] V. Philipps, B. P. Hejblum, M. Prague, D. Commenges and C. Proust-Lima, "Robust and efficient optimization using a Marquardt-Levenberg algorithm with R package marqLevAlg," *The R Journal* Vol. 13/2, December 2021 p 365-379.
- [3] B. Ribba, N. H. Holford, P. Magni, I. Trocóniz, I. Gueorguieva, P. Girard, C. Sarr, M. Elishmereni, C. Kloft and L. E. Friberg, "A review of mixed-effects models of tumor growth and effects of anticancer drug treatment used in population analysis.," *CPT: pharmacometrics & systems pharmacology*, 2014.
- [4] *Monolix, Lixoft SAS, Version 2019R1.*, 2019.
- [5] F. Nassiri, G. Tabatabai, K. Aldape and G. Zadeh, *Challenges and opportunities in meningiomas: recommendations from the International Consortium on Meningiomas. Neuro-Oncol. 21, i2-i3 (2019).*